https://doi.org/10.15407/ujpe71.7.607

A.V. KOROTUN [1, 2]

[1] National University Zaporizhzhia Politechnic
(64, Universytetska Str., Zaporizhzhia 69011; e-mail: andko@zp.edu.ua)
[2] G.V. Kurdyumov Institute for Metal Physics, Nat. Acad. of Sci. of Ukraine
(3, Academician Vernadsky Blvd., Kyiv 03142)

OPTICAL RESPONSE OF METALLIC NANOPARTICLES OF TOROIDAL SHAPE

The optical properties of toroidal-shaped metallic nanoparticles in a dielectric medium are investigated in the work. The equivalent oblate spheroid approach has been used to obtain the frequency dependences of the absorption and scattering cross-sections, as well as the diagonal components of the polarizability tensor and electric field enhancement tensor. The numerical results for the corresponding frequency dependencies are analyzed. The fact of the anomalously large splitting of the absorption and scattering cross-section maxima, which distinguishes toroidal particles from the whole class of the axisymmetric nanoparticles, has been established. The size dependences of the transverse and longitudinal frequencies of surface plasmonic resonance have been determined in the dissipation-free approximation. The influence of the toroidal shape and material of the nanoparticles as well as the material of the surrounding medium on their optical response is studied.

K e y w o r d s: toroidal metallic nanoparticle, absorption cross-section, polarizability tensor, dielectric tensor, equivalent spheroid approach, surface plasmonic resonance.

1. Introduction

The electronic and optical properties of nanoparticles are of considerable interest from the viewpoint of practical applications [1–6]. New nanofabrication methods and the use of templates make it possible to fabricate metallic nanostructures with complex shapes and unique properties [7–13]. The optical properties of metallic nanostructures are determined by their plasmonic resonances, which can depend significantly on their shape, composition, and dielectric medium properties [1–3, 5, 14–16]. For some nanoparticles, such as nanoshells [17–19] and nanorods [20, 21], the plasmonic energy can be tuned from the near-ultraviolet to the mid-infrared region of the spectrum. Such tunability has been used in many important applications such as chemical and biological sensing [22–25], optical manipulation of nanoparticles [26], plasmonic waveguides [27, 28], metamaterials [29], and biomedical applications [23].

Metallic nanoscale rings and toroids are interesting highly tunable plasmonic geometries with significant potential as a platform for chemical and biological sensing, as well as for exploiting magnetic effects at optical frequencies [30–35]. The optical properties of nanorings and toroidal nanoparticles were calculated using the boundary element method [36, 37], Green's dyadic tensor approach [38, 39], and the finite-difference time-domain (FDTD) method [40].

C i t a t i o n: Korotun A.V. Optical response of metallic nanoparticles of toroidal shape. *Ukr. J. Phys.* **71**, No. 7, 607 (2026). https://doi.org/10.15407/ujpe71.7.607.

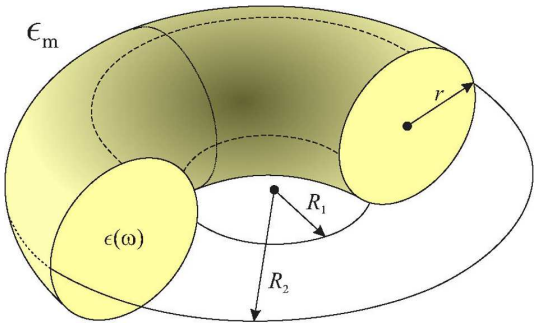

Fig. 1. Geometry of the problem

In Ref. [41] the plasmonic and optical properties of metallic nanoscale toroids are investigated using the plasmonic hybridisation model [42, 43], and it is shown that the plasmonic resonances in a nanotoroid arise from the hybridization of primitive plasmonic modes, which can be described as toroidal harmonics. However, this approach is mathematically cumbersome and does not allow us to obtain expressions for some optical characteristics (for example, the expressions for the diagonal components of the polarizability tensor and field enhancement tensor). In this respect, the equivalent spheroid approach, proposed in [44] and developed in a series of papers [21, 45–49], is simpler and more convenient for studying the optical properties of metallic nanostructures of different shapes. In this connection, the above approach is used in this work to study the spectral characteristics of toroidal nanoparticles.

2. Mathematical Model

2.1. Absorption and scattering cross-sections and polarizability tensor

Let the toroidal metallic nanoparticle be in a medium with the permittivity $\epsilon_{\rm m}$, with the radius of the hole R_1, the radius of the outer circle R_2, and r is the radius of the "tube" of the torus (Fig. 1).

The initial relations for the analysis will be the formulas for the absorption and scattering cross-sections

$$C_{\rm abs} = \frac{\omega}{c}\sqrt{\epsilon_{\rm m}}\,{\rm Im}\left(\frac{2}{3}\alpha_{\perp} + \frac{1}{3}\alpha_{\parallel}\right), \tag{1}$$

$$C_{\rm sca} = \frac{1}{6\pi}\left(\frac{\omega}{c}\right)^4 \epsilon_{\rm m}^2\left(\frac{2}{3}|\alpha_{\perp}|^2 + \frac{1}{3}|\alpha_{\parallel}|^2\right), \tag{2}$$

where ω and c are the frequency of the electromagnetic wave and the speed of the electromagnetic wave, and $\alpha_{\perp(\parallel)}(\hbar\omega)$ are the diagonal components of the polarizability tensor for the toroidal nanoparticle, which are determined using the equivalent oblate spheroid approach. The essence of this approach is as follows. The optical characteristics of the toroidal nanoparticle (in particular, the transverse and longitudinal components of the polarizability) coincide with those of the equivalent oblate spheroid. In this case, the aspect ratio of the equivalent oblate spheroid (the effective aspect ratio) is related to the aspect ratio of the toroid by a relation, which will be obtained below. The indicated relation, in turn, follows from the condition of the equality between the ratios of the corresponding axial moments of inertia of the toroid and the equivalent oblate spheroid.

Thus, the expressions for the diagonal components of the polarizability of the toroidal metallic nanoparticle have the following form

$$\alpha_{\perp(\parallel)}(\hbar\omega) = V\frac{\epsilon^{\perp(\parallel)}(\hbar\omega) - \epsilon_{\rm m}}{\epsilon_{\rm m} + \mathcal{L}_{\perp(\parallel)}\left(\epsilon^{\perp(\parallel)}(\hbar\omega) - \epsilon_{\rm m}\right)}, \tag{3}$$

where V is the volume of the toroidal nanoparticle; $\mathcal{L}_{\perp(\parallel)}$ are the depolarization factors, which can be expressed in terms of the effective aspect ratio as follows

$$\mathcal{L}_{\parallel} = \frac{\varrho_{\rm eff}^2}{\left(\varrho_{\rm eff}^2+1\right)^{\frac{3}{2}}}\left(\sqrt{\varrho_{\rm eff}^2-1} + {\rm arctg}\,\frac{1}{\sqrt{\varrho_{\rm eff}^2-1}} - \frac{\pi}{2}\right),$$

$$\mathcal{L}_{\perp} = \frac{1}{2}\left(1 - \mathcal{L}_{\parallel}\right) \tag{4}$$

and the diagonal components of the dielectric tensor are

$$\epsilon^{\perp(\parallel)}(\hbar\omega) = \epsilon^{\infty} - \frac{\omega_p^2}{\omega\left(\omega + {\rm i}\gamma_{\rm eff}^{\perp(\parallel)}\right)}. \tag{5}$$

In formula (5), ω_p is the plasma frequency, ϵ^{∞} is the contribution of the interzone transitions into the permittivity of the metal, and $\gamma_{\rm eff}^{\perp(\parallel)}$ are the diagonal components of the effective relaxation rate tensor, which will be determined further.

2.2. Effective aspect ratio

The axial moments of inertia of the equivalent oblate spheroid

$$I_x^{\rm sph} = \frac{m_1}{5}\left(a^2+b^2\right), \quad I_z^{\rm sph} = \frac{2}{5}m_1a^2, \tag{6}$$

where m_1 is the mass of the spheroid, a and b are its major and minor semiaxes.

In turn, the axial moments of inertia of the toroid

$$I_x^{\rm tor} = \frac{2m_2}{\pi}\left(R_2^2 + (R_2 - 2r)^2\right), \tag{7}$$

$$I_z^{\rm tor} = m_2\left(\frac{3}{4}r^2 + R_2^2\right), \tag{8}$$

where m_2 is the mass of the toroid.

As indicated above, the relation between the equivalent aspect ratio

$$\varrho_{\rm eff} = \frac{a}{b} \tag{9}$$

and the aspect ratio

$$\varrho = \frac{R_2}{2r} \tag{10}$$

can be found from the following condition

$$\frac{I_x^{\rm sph}}{I_z^{\rm sph}} = \frac{I_x^{\rm tor}}{I_z^{\rm tor}}. \tag{11}$$

Since

$$\frac{I_x^{\rm sph}}{I_z^{\rm sph}} = \frac{1}{2} + \frac{1}{2\varrho_{\rm eff}^2} \tag{12}$$

and

$$\frac{I_x^{\rm tor}}{I_z^{\rm tor}} = \frac{2}{\pi}\frac{2\varrho^2 - 2\varrho + 1}{\frac{3}{16} + \varrho^2} \tag{13}$$

then, substituting the expressions (12) and (13) into formula (11), we finally obtain

$$\varrho_{\rm eff} = \left(\frac{4}{\pi}\frac{2\varrho^2 - 2\varrho + 1}{\varrho^2 + \frac{3}{16}} - 1\right)^{-1}. \tag{14}$$

2.3. Effective relaxation rate and surface plasmonic resonances

Let us assume that the relaxation processes in the toroidal nanoparticle are determined by three mechanisms: bulk and surface electron scattering and radiation damping. Therefore, the relations for the transverse and longitudinal effective relaxation rates take the following form

$$\gamma_{\rm eff}^{\perp(\parallel)} = \gamma_{\rm bulk} + \gamma_{\rm s}^{\perp(\parallel)} + \gamma_{\rm rad}^{\perp(\parallel)}, \tag{15}$$

where the bulk relaxation rate $\gamma_{\rm bulk} = {\rm const}$ for a specific metal, and the surface relaxation rate and the radiation damping rate are determined by the relations [49]

$$\gamma_{\rm s}^{\perp(\parallel)} = \mathscr{A}_{\perp(\parallel)}\frac{v_{\rm F}}{\ell_{\perp(\parallel)}}, \tag{16}$$

$$\gamma_{\rm rad}^{\perp(\parallel)} = \mathscr{B}_{\perp(\parallel)}\frac{v_{\rm F}}{\ell_{\perp(\parallel)}}. \tag{17}$$

In formulas (17) and (18) $v_{\rm F}$ is the Fermi velocity of electrons; $\ell_{\perp(\parallel)}$ are the effective electron mean free paths in the transverse and longitudinal directions

$$\ell_\perp = \ell_\parallel = 2r \tag{18}$$

the size-dependent and frequency-dependent functions have the following form

$$\mathscr{A}_{\perp(\parallel)} = \\ = \frac{9}{16}\frac{\mathcal{L}_{\perp(\parallel)}}{\epsilon_{\rm m} + \mathcal{L}_{\perp(\parallel)}(1 - \epsilon_{\rm m})}\left(\frac{\omega_p}{\omega}\right)^2 \mathscr{F}_{\perp(\parallel)}(\varrho_{\rm eff}), \tag{19}$$

$$\mathscr{B}_{\perp(\parallel)} = \frac{9V}{128\pi}\frac{\mathcal{L}_{\perp(\parallel)}}{\sqrt{\epsilon_{\rm m}\left[\epsilon^\infty + \left(\frac{1}{\mathcal{L}_{\perp(\parallel)}} - 1\right)\epsilon_{\rm m}\right]}} \times \\ \times \left(\frac{\omega_p}{c}\right)^3\left(\frac{\omega_p}{\omega}\right)^2 \mathscr{F}_{\perp(\parallel)}(\varrho_{\rm eff}), \tag{20}$$

where the volume of toroid

$$V = 2\pi^2 r^2 (R_2 - r) \tag{21}$$

and the size factors of the oblate spheroid

$$\mathscr{F}_\perp(\varrho_{\rm eff}) = \frac{\varrho_{\rm eff}\left(2\varrho_{\rm eff}^2 - 3\right)\sqrt{\varrho_{\rm eff}^2 - 1}}{2(\varrho_{\rm eff}^2 - 1)^{\frac{3}{2}}} + \\ + \frac{\left(4\varrho_{\rm eff}^2 - 3\right)\ln\left(\varrho_{\rm eff} + \sqrt{\varrho_{\rm eff}^2 - 1}\right)}{2(\varrho_{\rm eff}^2 - 1)^{\frac{3}{2}}}, \tag{22}$$

$$\mathscr{F}_\parallel(\varrho_{\rm eff}) = \frac{\varrho_{\rm eff}\left(2\varrho_{\rm eff}^2 - 1\right)\sqrt{\varrho_{\rm eff}^2 - 1}}{(\varrho_{\rm eff}^2 - 1)^{\frac{3}{2}}} - \\ - \frac{\ln\left(\varrho_{\rm eff} + \sqrt{\varrho_{\rm eff}^2 - 1}\right)}{(\varrho_{\rm eff}^2 - 1)^{\frac{3}{2}}}. \tag{23}$$

As is well known, the condition for the excitation of surface plasmonic resonances is that the real part of the denominator of expression (3) be equal to zero. Taking into account formula (5) in the dissipation-free approximation ($\gamma_{\rm eff}^{\perp(\parallel)} \to 0$), the size

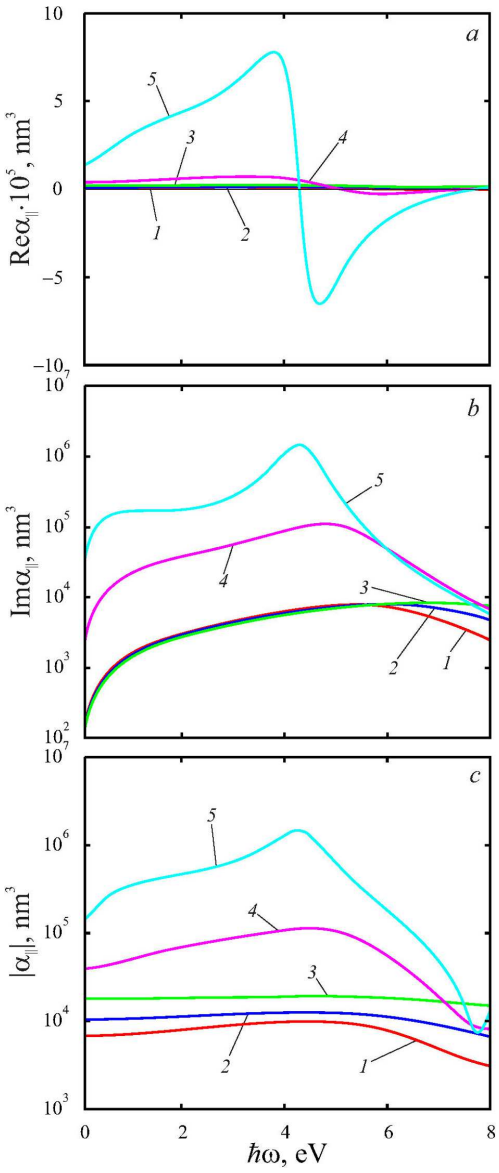

Fig. 2. The frequency dependencies for the real (a) and imaginary (b) parts, as well as the magnitude (c) of the longitudinal component of the polarizability tensor of the toroidal silver nanoparticle in Teflon: *1* – $r = 5$ nm, $R_2 = 40$ nm; *2* – $r = 5$ nm, $R_2 = 60$ nm; *3* – $r = 5$ nm, $R_2 = 100$ nm; *4* – $r = 10$ nm, $R_2 = 60$ nm; *5* – $r = 20$ nm, $R_2 = 60$ nm

dependences of the transverse and longitudinal resonance frequencies have the following form

$$\omega_{sp}^{\perp(\parallel)}\left(\varrho_{\text{eff}}\right) = \frac{\omega_p}{\sqrt{\epsilon^{\infty} + \frac{1-\mathcal{L}_{\perp(\parallel)}}{\mathcal{L}_{\perp(\parallel)}}\epsilon_{\text{m}}}}. \tag{24}$$

In turn, the diagonal components of the electric-field enhancement tensor are determined by the relations

$$\mathscr{G}_{\perp(\parallel)} = \\ = \frac{\epsilon_1^{\perp(\parallel)\,2} + \epsilon_2^{\perp(\parallel)\,2}}{\left[\mathcal{L}_{\perp(\parallel)}\left(\epsilon_1^{\perp(\parallel)} - \epsilon_{\text{m}}\right) + \epsilon_{\text{m}}\right]^2 + \left[\mathcal{L}_{\perp(\parallel)}\epsilon_2^{\perp(\parallel)}\right]^2}. \tag{25}$$

In the following, expressions (1)–(3) and (24), (25) taking into account formulas (4), (5), (14)–(23) will be used to obtain the numerical results.

2.4. Results of the calculation and their discussion

The calculations of the real and imaginary parts, as well as the magnitudes of the diagonal components of the polarizability tensor, as well as the absorption and scattering cross-sections have been performed for the toroidal nanoparticles of different sizes, made of different metals and embedded in different dielectric media. The diagonal components of the electric field enhancement tensor for the toroidal, disk-shaped, and spheroidal nanoparticles were compared. The data required for the calculations, are given in Tables 1 and 2.

The frequency dependences of the real and imaginary parts, as well as the magnitudes of the longitudinal and transverse components of the polarizability tensor are presented in Figs. 2 and 3. Let us point out that, as in the case of nanoparticles of other

Table 1. **Parameters of metals [21, 48]**

Metal	Parameter			
	r_s/a_0	m^*/m_e	ϵ^{∞}	γ_{bulk}, 10^{13} s^{-1}
Pd	4.00	0.37	2.52	13.9
Pt	3.27	0.54	4.42	10.52
Ag	3.02	0.96	3.70	2.50
Au	3.01	0.99	9.84	3.45
Cu	2.11	1.49	12.03	3.70

Table 2. **Parameters of metals [21, 48]**

Matrix	Air	CaF_2	Teflon	Al_2O_3	TiO_2
ϵ_{m}	1.00	1.54	2.30	3.13	4.00

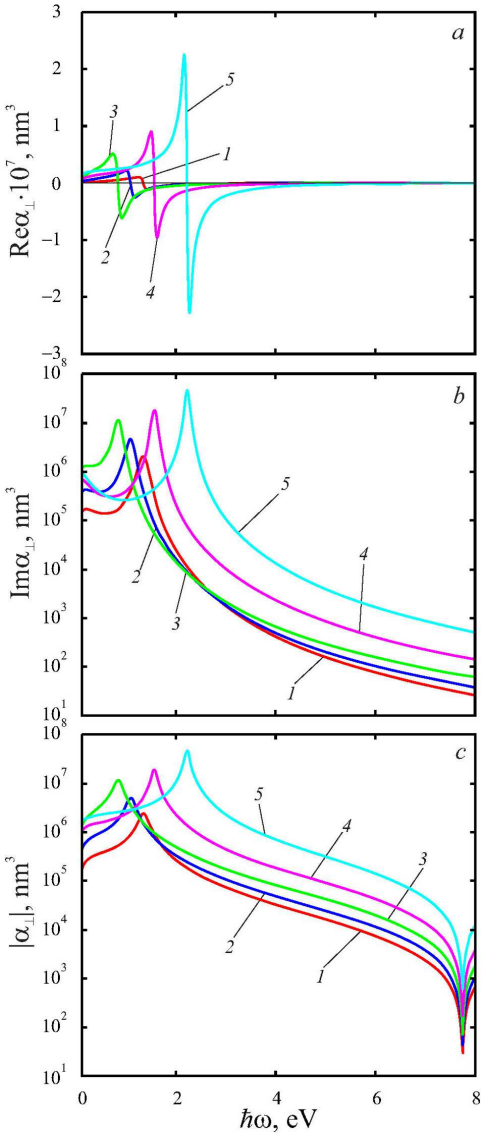

Fig. 3. The frequency dependencies for the real (a) and imaginary (b) parts, as well as the magnitude (c) of the transverse component of the polarizability tensor of the toroidal silver nanoparticle in Teflon under the same parameters as in Fig. 2

shapes [21, 46–49], the functions $\mathrm{Re}\,\alpha_{\perp(\parallel)}(\hbar\omega)$ for the toroidal particles are alternating function, whereas $\mathrm{Im}\alpha_{\perp(\parallel)}(\hbar\omega) > 0$. In addition, $\max\{\mathrm{Im}\,\alpha_{\parallel}\}$ are situated in the ultraviolet region of the spectrum, while $\max\{\mathrm{Im}\,\alpha_{\perp}\}$ are situated in the near infrared and visible regions. The amplitudes of the maxima of the imaginary part of the transverse component significantly exceed the corresponding values for the longitudinal component. Moreover, increasing the aspect ratio (the curves in the sequence $1 \to 2 \to 3$ and $5 \to 4 \to 2$) leads to the "blue" shift of $\max\{\mathrm{Im}\alpha_{\parallel}\}$ and the "red" shift of $\max\{\mathrm{Im}\alpha_{\perp}\}$, and hence an increase in the splitting of the surface plasmonic resonance frequency. It should be pointed out that of all types of nanoparticles with the axial symmetry, the optical (plasmonic) properties of which were investigated in our previous works – cylinder, spherocylinder, disk, biconus, and bipyramid [21, 46–49], the splitting of resonance frequencies is greatest for the toroidal particles. This is due to the influence of the size factor, namely the behavior of the depolarization factors with increasing aspect ratio ($\mathcal{L}_{\perp} \to 0$, $\mathcal{L}_{\parallel} \to 1$). Thus, for the greatest aspect ratio in the considered cases (curves *3* in Figs. 2, *b* and 3, *b*), the splitting of the resonant frequencies is $\Delta\omega_{sp} = \omega_{sp}^{\parallel} - \omega_{sp}^{\perp} > 5$ eV.

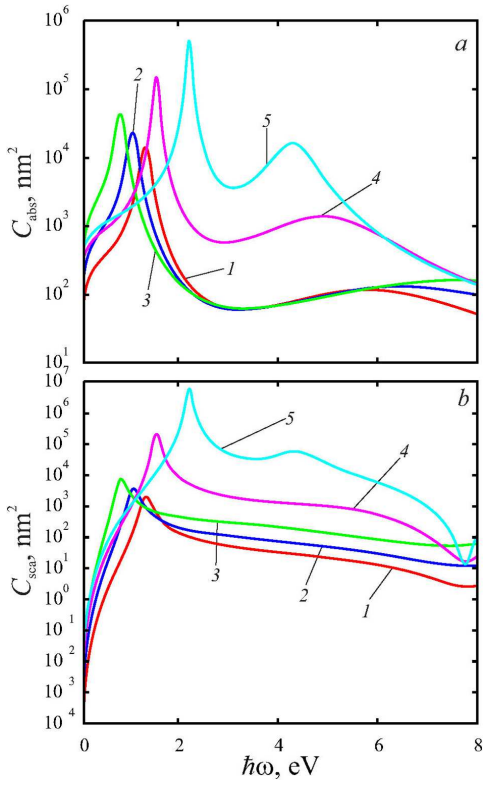

Fig. 4. The frequency dependencies for the absorption cross-sections (a) and scattering cross-section (b) of the silver nanotoroid in Teflon under the same parameters as in Fig. 2

The described behavior of the frequency dependences of the longitudinal and transverse polarizabil-

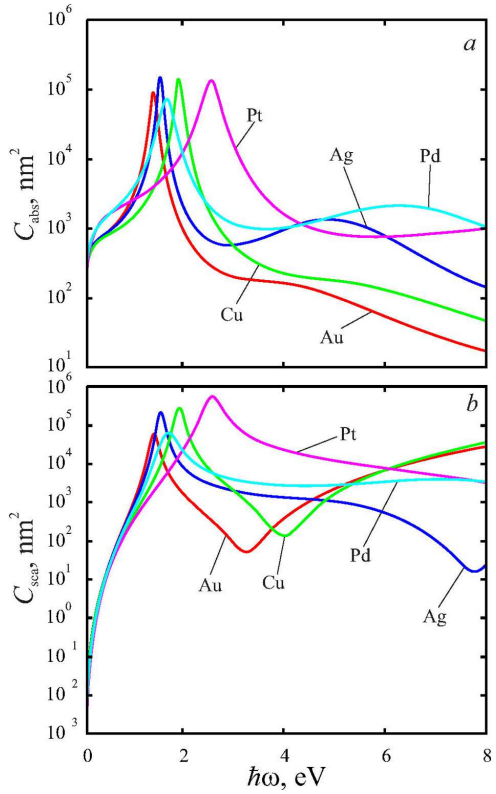

Fig. 5. The frequency dependencies for the absorption cross-section (a) and scattering cross-section (b) of the toroidal nanoparticles of different metals in Teflon (r = 10 nm, R_2 = = 60 nm)

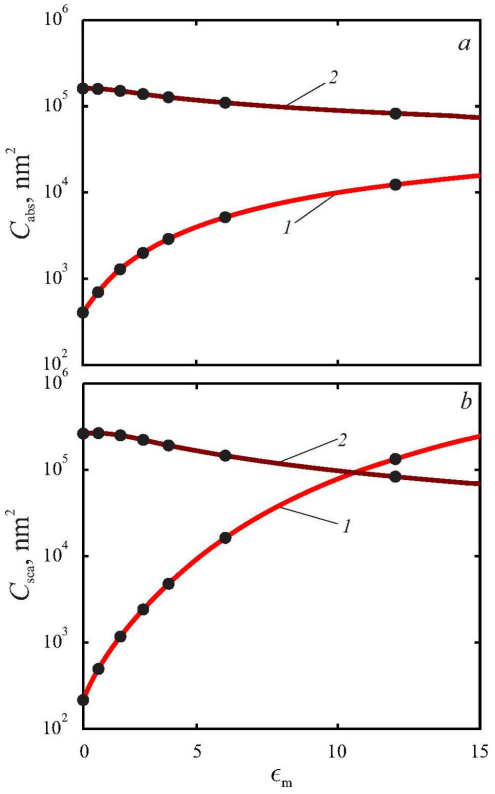

Fig. 6. The dependencies of the absorption cross-section (a) and scattering cross-section (b) of toroidal Ag nanoparticles (r = 10 nm, R_2 = 60 nm) at the frequencies of the transverse SPR (curve *1*) and longitudinal SPR (curve *2*) on the permittivity of the surrounding medium. The points correspond to the permittivities of the dielectrics given in Table 2

ity correlates with the behavior of the corresponding curves for the absorption and scattering cross-sections (Fig. 4). The maxima of the indicated curves are also located in different spectral ranges, and the amplitudes of the maxima corresponding to transverse surface plasmonic resonances, significantly exceed those corresponding to longitudinal resonances up to the complete disappearance of the latter in the $C_{\rm sca}\,(\hbar\omega)$ curves.

The frequency dependences of the absorption and scattering cross-sections of toroidal nanoparticles of different metals are shown in Fig. 5. Let us point out that the behavior of the second maxima of the absorption and scattering cross-sections (at the frequency $\omega_{sp}^{\parallel}$) for nanoparticles of other metals is similar to that observed for silver toroidal nanoparticles. In turn, $\max\{C_{\rm abs}\}$ and $\max\{C_{\rm sca}\}$ at the frequency $\omega_{sp}^{\perp}$ for particles of considered metals are situated in the near-infrared and visible parts of the spectrum, which differs significantly from the cases of other nanoparticles, which have axial symmetry. The reason for this shift of the maxima is also the influence of the size factor, namely, the small value of the depolarization factor $\mathcal{L}_{\perp}$, which leads to a significant "red" shift of $\omega_{sp}^{\perp}$ for toroidal nanoparticles of the considered composition.

The dependences of the absorption and scattering cross-sections on the permittivity of the dielectric medium surrounding the silver toroidal nanoparticle, calculated at the frequencies of the transverse and longitudinal surface plasmonic resonances, are shown in Fig. 6. The general trend is for $C_{\rm abs}$ and $C_{\rm sca}$ to decrease at the frequency $\omega_{sp}^{\perp}$ and to increase at the frequency $\omega_{sp}^{\parallel}$ as the permittivity increases. Nevertheless, for the permittivities of the dielectrics used in practice, $C_{\rm abs(sca)}\left(\omega_{sp}^{\perp}\right) > C_{\rm abs(sca)}\left(\omega_{sp}^{\parallel}\right)$. It should

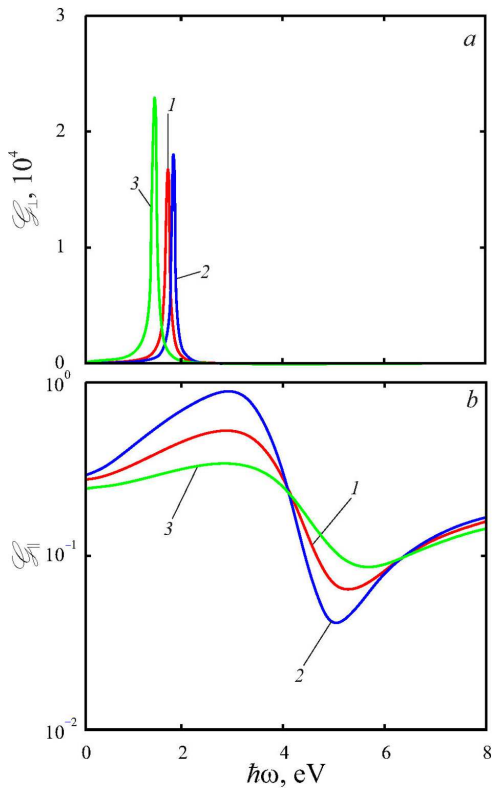

Fig. 7. Comparison of the frequency dependencies of the transverse (a) and longitudinal (b) components of the electric fields enhancement tensor for Ag nanoparticles in Teflon, having different shapes: *1* – oblate spheroid; *2* – disk; *3* – toroid, with the same longitudinal and transverse dimensions ($a_l = 10$ nm, $b_t = 60$ nm)

also be pointed out that the indicated results confirm the strong dependence of the optical response of nanoparticles of different shapes on the properties of the surrounding dielectric medium.

The curves of the frequency dependencies of the diagonal components of the electric field enhancement tensor for toroidal, disk-shaped, and spheroidal nanoparticles with the same longitudinal (the disk height, the doubled minor semiaxis of the oblate spheroid, and the radius of the toroid tube) and transverse (the diameter of the disk base, the doubled major semiaxis of the spheroid, and the outer radius of the toroid) sizes are presented in Fig. 7. Let us point out that $\mathscr{G}_\perp \gg \mathscr{G}_\parallel$, and $\mathscr{G}_\parallel < 1$ for all nanoparticle shapes under consideration. In addition, the amplitude of the maximum of the transverse component of the enhancement tensor grows in the order of nanoparticle shapes "oblate spheroid → disk → toroid", and $\max\{\mathscr{G}_\perp\}$ itself for the toroidal nanoparticle is reached at the frequencies lower than those for the disk and oblate spheroid.

3. Conclusions

The expressions for the frequency dependences of the diagonal components of the polarizability tensor and field enhancement tensor, together with the absorption and scattering cross-sections, are obtained in the framework of the equivalent spheroid approach.

It is shown that the maxima of the imaginary part of the longitudinal polarizability are located in the near-ultraviolet region of the spectrum, while the maxima of the imaginary part of the transverse polarizability are located in the near-infrared and visible regions. Thus, the toroidal nanoparticles are characterized by an anomalously large splitting of the plasmonic resonance, which allows them to occupy a special position among other axisymmetric particles.

It is demonstrated that the maxima of the absorption and scattering cross-sections at the frequencies of the longitudinal surface plasmonic resonance have much smaller amplitude than the maxima corresponding to the transverse resonance. This, in turn, means that these maxima do not appear on some scattering cross-section curves.

It was found that the small value of the transverse depolarization factor results in the shift of the corresponding maxima of the absorption and scattering cross-sections of the toroidal nanoparticles of different plasmonic metals toward the near-infrared and visible regions of the spectrum compared to the particles of other shapes.

The decrease and increase of the absorption and scattering cross-sections at the frequencies of the transverse/longitudinal surface plasmonic resonance with increasing permittivity of the surrounding dielectric confirms the sensitivity of the optical responses of toroidal nanoparticles to changes in the matrix properties.

The results of the calculations of the transverse and longitudinal components of the electric field enhancement tensor for the nanoscale toroids, disks, and oblate spheroids with the same transverse and longitudinal dimensions indicate the absence of field enhancement in the longitudinal direction for the particles of the considered shapes and the presence of

significant enhancement in the transverse direction, which increases in the sequence of shapes "oblate spheroid → disk → toroid".

1. P.K. Jain, K.S. Lee, I.H. El-Sayed, M.A. El-Sayed. Calculated absorption and scattering properties of gold nanoparticles of different size, shape, and composition: Applications in biological imaging and biomedicine. *J. Phys. Chem. B* **110**, 7238 (2006).
2. S.A. Maier. *Plasmonics: Fundamentals and Applications* (Springer, 2007).
3. M.L. Dmytruk, S.Z. Malynych. Surface plasmon resonances and their manifestation in the optical properties of nanostructures of noble metals. *Ukr. J. Phys.* **9**, 3 (2014/2019).
4. M. Sukharev, A. Nitzan. Optics of exciton-plasmon nanomaterials. *J. Phys.: Condens. Matter.* **29**, 443003 (2017).
5. A.O. Koval, A.V. Korotun, Yu.A. Kunytskyi, V.A. Tatarenko, I.M. Titov. *Electrodynamics of Plasmon Effects in Nanomaterials* (Naukova Dumka, 2021).
6. U. Ulusoy. A review of particle shape effects on material properties for various engineering applications: From macro to nanoscale. *Minerals* **13**, 91 (2023).
7. J.C. Garno, C.D. Zangmeister, J.D. Batteas. Directed electroless growth of metal nanostructures on patterned self-assembled monolayers. *Langmuir* **23**, 7874 (2007).
8. S.B. Ulapane, N.J.B. Kamathewatta, H.M. Ashberry, C.L. Berrie. Controlled electroless deposition of noble metals on silicon substrates using self-assembled monolayers as molecular resists to generate nanopatterned surfaces for electronics and plasmonics. *ACS Appl. Nano Mater.* **2**, 7114 (2019).
9. Q. Huo, J.G. Worden. Monofunctional gold nanoparticles: Synthesis and applications. *J. Nanopart. Res.* **9**, 1013 (2007).
10. K. Mahato, S. Nagpal, M.A. Shah, A. Srivastava, P.K. Maurya, S. Roy, A. Jaiswal, R. Singh, P. Chandra. Gold nanoparticle surface engineering strategies and their applications in biomedicine and diagnostics. *Biotech.* **9**, 57 (2019).
11. P. Kumar, C. Verma. *Surface-Functionalized Nanomaterials: Environmental, Energy Storage, Energy Conversion Applications* (De Gruyter, 2025).
12. S. Bidault, F.J.G. de Abajo, A. Polman. Plasmon-based nanolenses assembled on a well-defined DNA template. *J. Am. Chem. Soc.* **130**, 2750 (2008).
13. Y. Yang, Y. Jeon, Z. Dong *et al.* Nanofabrication for nanophotonics. *ACS Nano* **19**, 12491 (2025).
14. K.L. Kelly, E. Coronado, L.L. Zhao, G.C. Schatz. The optical properties of metal nanoparticles: The influence of size, shape, and dielectric environment. *J. Phys. Chem. B* **107**, 668 (2003).
15. N.J. Halas. Playing with plasmons: Tuning the optical resonant properties of metallic nanoshells. *MRS Bulletin* **30**, 362 (2005).
16. M.P. Mcoyi, K.T. Mpofu, M. Sekhwama, P. Mthunzi-Kufa. Developments in localized surface plasmon resonance. *Plasmonics* **20**, 5481 (2025).
17. V.V. Kulish, P.M. Tomchuk. Optical properties of metal nanotubes and metal nanoshells. *Surf. Sci.* **602**, 1045 (2008).
18. R.D. Averitt, D. Sarkar, N.J. Halas. Plasmon resonance shifts of Au-coated Au_2S nanoshells: Insight into multicomponent nanoparticle growth. *Phys. Rev. Lett.* **78**, 4217 (1997).
19. A.V. Korotun, A.A. KovalпїS, I.N. Titov. Optical absorption of a composite based on bilayer metal–dielectric spherical nanoparticles. *J. Appl. Spectrosc.* **87**, 240 (2020).
20. S. Link, M.B. Mohamed, M.A. El-Sayed. Simulation of the optical absorption spectra of gold nanorods as a function of their aspect ratio and the effect of the medium dielectric constant. *J. Phys. Chem. B* **103**, 3073 (1999).
21. A.V Korotun, Ya.V. Karandas, V.I. Reva. Analytical theory of plasmon effects in rod-like metal nanoparticles. The equivalent-spheroid model. *Ukr. J. Phys.* **67**, 849 (2023).
22. S. Lal, S. Link, N.J. Halas. Nano-optics from sensing to waveguiding. *Nature Photon* **1**, 641 (2007).
23. S.M.N.S. Kumari, X.T. Suryabai. Sensing the future – frontiers in biosensors: Exploring classifications, principles, and recent advances. *ACS Omega* **9**, 48918 (2024).
24. P. Zijlstra, M. Orrit, A.F. Koenderink. *Metal Nanoparticles for Microscopy and Spectroscopy* (Springer, 2024).
25. N. Kyvelos, N.A. Mortensen, X. Zheng, C. Tserkezis. Self-similar plasmonic nanolenses: Mesoscopic ensemble averaging and chiral lightпїSmatter interactions. *J. Phys. Chem. C* **129**, 3635 (2025).
26. R.P.M. Höller, I.J. Jahn, D. Cialla-May, M. Chanana. Biomacromolecular-assembled nanoclusters: Key aspects for robust colloidal SERS sensing. *ACS Appl. Mater. Interfaces* **12**, 57302 (2020).
27. S.A. Maier, H.A. Atwater. Plasmonics: Localization and guiding of electromagnetic energy in metal/dielectric structures. *J. Appl. Phys.* **98**, 011101 (2005).
28. A.G. Bracamonte. *Development of Advanced Nano-Optics for Miniaturized Optical Set-Ups and Instrumentation* (CRC Press, 2025).
29. A. Ahmadivand, B. Gerislioglu. Photonic and plasmonic metasensors. *Laser and Photonics Reviews* **16**, 2100328 (2021).
30. J. Aizpurua, P. Hanarp, D.S. Sutherland, M. Kall, G.W. Bryant, F.J. Garcia de Abajo. Optical properties of gold nanorings. *Phys. Rev. Lett.* **90**, 057401 (2003).
31. S.I. Bozhevolnyi, V.S. Volkov, E. Devaux, J.-Y. Laluet, T.W. Ebbesen. Channel plasmon subwavelength waveguide components including interferometers and ring resonators. *Nature* **440**, 508 (2006).
32. E.M. Larsson, J. Alegret, M. Kall, D.S. Sutherland. Sensing characteristics of NIR localized surface plasmon resonances in gold nanorings for application as ultrasensitive biosensors. *Nano Lett.* **7**, 1256 (2007).

33. M. Wang, H. Cai, Z. Su, Z. Yang, G. Ding, F. Zang. Narrow-Gap-Integrated ringaArrays (GRA) as ultrahigh field-enhancement optical resonators. *Adv. Funct. Mater.* **35**, 2417739 (2025).
34. C. Liu, S. Gu, M. Sun, Y. Zhang, J. Han. Theoretical investigation of terahertz spoof surface-plasmon-polariton devices based on ring resonators. *Photonics* **12**, 70 (2025).
35. X. Luo, R. Tan, Q. Li, J. Chen, Y. Xie, J. Peng, M. Zeng, M. Jiang, C. Wu, Y. He. High-sensitivity long-range surface plasmon resonance sensing assisted by gold nanoring cavity arrays and nanocavity coupling. *Phys. Chem. Chem. Phys.* **25**, 9273 (2023).
36. F.J. Garcia de Abajo, J. Aizpurua. Numerical simulation of electron energy loss near inhomogeneous dielectrics. *Phys. Rev. B* **56**, 15873 (1997).
37. J. Aizpurua, L. Blanco, P. Hanarp, D.S. Sutherland, M. Kall, G.W. Bryant, F.J.G. de Abajo. Light scattering in gold nanorings. *Quant. Spectrosc. Radiat. Transf.* **89**, 11 (2004).
38. A. Mary, A. Dereux, T.L. Ferrell. Localized surface plasmons on a torus in the nonretarded approximation. *Phys. Rev. B* **72**, 155426 (2005).
39. A. Mary, D.M. Koller, A. Hohenau, J.R. Krenn, A. Bouhelier, A. Dereux. Optical absorption of torus-shaped metal nanoparticles in the visible range. *Phys. Rev. B* **76**, 245422 (2007).
40. F. Hao, P. Nordlander, M.T. Burnett, S.A. Maier. Enhanced tunability and linewidth sharpening of plasmon resonances in hybridized metallic ring/disk nanocavities. *Phys. Rev. B* **76**, 245417 (2007).
41. C.M. Dutta, T.A. Ali, D.W. Brandl, T.-H. Park, P. Nordlander. Plasmonic properties of a metallic torus. *J. Chem. Phys.* **129**, 419 (2003).
42. E. Prodan, C. Radloff, N.J. Halas, P. Nordlander. A hybridization model for the plasmon response of complex nanostructures. *Science* **302**, 419 (2003).
43. E. Prodan, P. Nordlander. Plasmon hybridization in spherical nanoparticles. *J. Chem. Phys.* **120**, 5444 (2004).
44. D. Constantin. Why the aspect ratio? Shape equivalence for the extinction spectra of gold nanoparticles. *Eur. Phys. J. E* **38**, 116 (2015).
45. A.V. Korotun, N.I. Pavlyshche. Optical absorption of a composite with randomly distributed metallic inclusions of various shapes. *Funct. Mat.* **29**, 567 (2022).
46. A.V. Korotun. Plasmonic phenomena in biconical and bipyramidal metal nanoparticles. *Ukr. J. Phys.* **68**, 695 (2023).
47. A.V. Korotun. More on the size effects on the spectral figure of merit and enhancement of the local fields in the neighborhood of biconical and bipyramidal metallic nanoparticles. *Low Temp. Phys.* **51**, 133 (2025).
48. N.I. Pavlyshche, A.V. Korotun, V.P. Kurbatsky, V.I. Reva. Plasmon phenomena in metal-dielectric nanodiscs. An equivalent-spheroid approach. *Ukr. J. Phys.* **70**, 263 (2025).
49. N.I. Pavlyshche, A.V. Korotun, V.P. Kurbatsky, R.Yu. Korolkov. Plasmon phenomena in metal-dielectric nanodiscs. An equivalent-spheroid approach. *Funct. Mater.* **32**, 108 (2025).

Received 17.12.25

А.В. Коротун

ОПТИЧНИЙ ВІДГУК МЕТАЛЕВИХ НАНОЧАСТИНОК ТОРОЇДАЛЬНОЇ ФОРМИ

У роботі досліджено оптичні властивості металевих наночастинок тороїдальної форми, що містяться в діелектричному середовищі. Для отримання частотних залежностей перерізів поглинання й розсіяння, а також діагональних компонент тензорів поляризовності й підсилення електричних полів, використано підхід еквівалентного сплюснутого сфероїда. Аналізуються чисельні результати для відповідних частотних залежностей. Встановлено факт аномально великого розщеплення максимумів перерізів поглинання й розсіяння, що виділяє тороїдальні частинки з усього класу аксіально-симетричних наночастинок. У бездисипативному наближенні визначено розмірні залежності поперечної та поздовжньої частот поверхневого плазмонного резонансу. Вивчено вплив тороїдальної форми й матеріалу наночастинок, а також матеріалу навколишнього середовища на їхній оптичний відгук.

Ключові слова: тороїдальна металева наночастинка, переріз поглинання, тензор поляризовності, діелектричний тензор, підхід еквівалентного сфероїда, поверхневий плазмонний резонанс.